

# Australian Orbit Determination of Manoeuvring GEO Satellites

Mark Rutten<sup>1</sup>, Cameron Webb<sup>2</sup>, Sergey Kharabash<sup>2</sup>, Kruger White<sup>2</sup>

<sup>1</sup>*In Track Solutions*

<sup>2</sup>*Defence Science and Technology Group*

## ABSTRACT

Australia's Defence Science & Technology Group (DSTG) is developing an experimental space domain awareness (SDA) system to inform the evolution of Australia's operational SDA capability. The Research and Development Space Target Awareness and Response (RED STAR) system includes a multi-sensor orbit determination data processing pipeline, which accepts data from several different sensor types, performs data curation, and executes orbit determination to form orbital state vectors that are published to a shared repository for exchange with space operators.

An ever-present challenge for orbit determination of active satellites is managing the unpredictable motion of manoeuvring satellites. DSTG has developed an orbit determination algorithm that is based on multiple-model filtering, which provides the ability to estimate the orbit throughout the duration of a manoeuvre. An estimate of an object's orbit is produced at every observation time along with a probability of manoeuvre, which can be used as a manoeuvre indicator. A multiple-model smoother then uses the output from the multiple-model filter to calculate details of the manoeuvre, such as manoeuvre time and delta-V. DSTG's orbit determination algorithm can process observation data from multiple sensor locations and sensor types, including ground-based and space-based optical data, deep-space radar and passive RF. At every step the algorithm carefully accounts for the uncertainties in the sensor observation data and generates state and parameter uncertainties (covariance).

This paper describes DSTG's orbit determination algorithm for manoeuvring satellites. The performance of the algorithm is demonstrated for a simulated scenario in which a Geosynchronous Earth Orbit (GEO) satellite conducts known manoeuvres. Details are provided on the relationship between this algorithm and other parts of the RED STAR system, which include data ingestion, data curation and initial orbit determination (IOD). Publication of the resulting state vectors and manoeuvre notifications enables information to be exchanged with external organisations for distributed space operations.

## 1. INTRODUCTION

Australia has growing strategic and operational interests in monitoring the space domain. As both Defence and national security operations increasingly rely on space-based capabilities—such as satellite communications, intelligence, surveillance and reconnaissance (ISR), and position, navigation, and timing (PNT) services—assured access to the space environment has become critical. These services are essential not only for military operations conducted by the Australian Defence Force (ADF), both domestically and abroad, but also for supporting vital civil systems. To protect these assets and ensure operational resilience, Australia requires space domain awareness (SDA) of objects and activities in space.

SDA encompasses a wide range of activities aimed at understanding and predicting the behaviour of objects and activities in space. The scope of SDA encompasses the detection and tracking of space objects, integration of multi-modal sensor data, orbit determination and prediction, identification and estimation of object manoeuvres, analysis of on-orbit behaviours, and the provision of threat indications and warnings.

Australia is developing a space domain awareness system to monitor activity in Earth orbit and support Defence and national security operations. Two SDA sensors are located and operated in Australia and form a part of the US Space Surveillance Network (SSN). The C-Band Space Surveillance Radar performs tracking of Low Earth Orbit (LEO) objects contributing to collision avoidance, satellite cataloguing, and launch tracking [1]. The Space Surveillance Telescope (SST) is an advanced optical sensor capable of detecting and tracking objects in Geosynchronous Earth Orbit (GEO) and beyond [2]. Construction of the Australian Deep-space Advanced Radar Capability (DARC) was

completed in December 2024 with mission system integration and test activities being conducted before operations are scheduled to commence by 2026 [3, 4].

Australia contributes to the United States' Joint Commercial Operations (JCO), a program led by the U.S. Space Force that leverages commercial industry capabilities to enhance space domain awareness [5]. The JCO operates through a tri-regional structure encompassing the Americas, Pacific, and Meridian cells, each supporting SDA. Within this framework, Sprint Advanced Concept Training (SACT) exercises have provided an experimental environment to assess and integrate emerging commercial data sources, analytical tools, and operational concepts [6]. The Space Domain Awareness Technology, Applications and Processing (SDA TAP) Lab is an initiative established to accelerate the development, testing, and integration of innovative SDA tools and technologies focused on addressing defined SDA problems [7, 8].

In addition to Australia's Defence SDA efforts, the Australian Space Agency is advancing civil space monitoring capabilities to promote the safety and sustainability of space traffic [9].

The Defence Science and Technology Group (DSTG) is the Australian Government's lead agency for applying science and technology to safeguard national defence and security. DSTG plays a key role in driving innovation, developing advanced technical solutions, and providing expert advice to shape Defence capabilities.

DSTG's space program integrates various research efforts to support space capabilities for Defence. Launched on 15 March 2025, the Buccaneer Main Mission (BMM) 6U cubesat carries a high frequency receiver for analysis of radiofrequency propagation through the ionosphere [10]. DSTG's Cortex system performs satellite spectrum monitoring to support planning for Defence satellite network operations [11]. A DSTG-led team has developed an experimental SDA system known as the Research and Development Space Target Awareness and Response system (RED STAR) [12].

This paper discusses manoeuvring satellites and then describes algorithms that have been developed for detecting and estimating space object manoeuvres using SDA sensor observation data. The algorithms are implemented as part of DSTG's RED STAR effort. Results are presented with an example simulation of satellite manoeuvres conducted in the Geosynchronous Earth Orbit (GEO) regime.

## **2. RED STAR OVERVIEW**

RED STAR serves as a research and prototyping environment to support the development of Australia's SDA capabilities [12]. Figure 1 shows the architecture of RED STAR. Designed to be modular and agile, RED STAR integrates data from a wide range of SDA sources including the Unified Data Library (UDL), catalogues such as space-track.org, various information sources and data sources such as from radar and optical sensors. The system supports both real-time sensor feeds and simulated data, enabling hybrid "sim-over-live" testing.

At its core, RED STAR operates as an integration and processing platform, accepting data from external sources and from the DSTG SDA Sensing module. An SDA Data Curation module performs normalisation and monitors incoming data, including data quality statistics, to maintain consistency for subsequent processing. Key functions of the SDA Algorithms module include multi-sensor orbit determination and the topic of this paper: manoeuvre detection and estimation. The SDA Modelling, Simulation and Analysis module comprises tools to allow DSTG scientists and engineers to test new algorithms and evaluate SDA scenarios in a controlled environment. In this paper, simulated data comprising spacecraft performing manoeuvres and an SDA sensor observing the spacecraft was fed to the manoeuvre detection and estimation algorithms for evaluation. SDA Intelligence Analytics performs integration and fusion of information about space entities in addition to permitting the description and communication of relationships between entities in orbit and on Earth.

Components of RED STAR are built as a cloud-native, containerised architecture with user interfaces designed for visualisation and decision support. The SDA Data Management module known as the Technology Research Environment for Knowledge of space (TREK) serves as the foundational layer that ensures reliable, consistent, and accessible data across RED STAR modules. An SDA Repository known as the Research and Development Repository

of Space Environment (RED ROSE) is used for storage of unprocessed and processed data which may be accessed via Representational State Transfer Application Programming Interfaces (REST APIs).

RED STAR is a science and technology testbed, actively shaped by SDA research and development needs that are raised during engagement with stakeholders in Defence, government, international partners, industry and academia. Through RED STAR, DSTG is building a scientific foundation for future SDA acquisitions, helping gather SDA evidence to make informed decisions about how Defence monitors and responds to activities in the increasingly contested space domain.

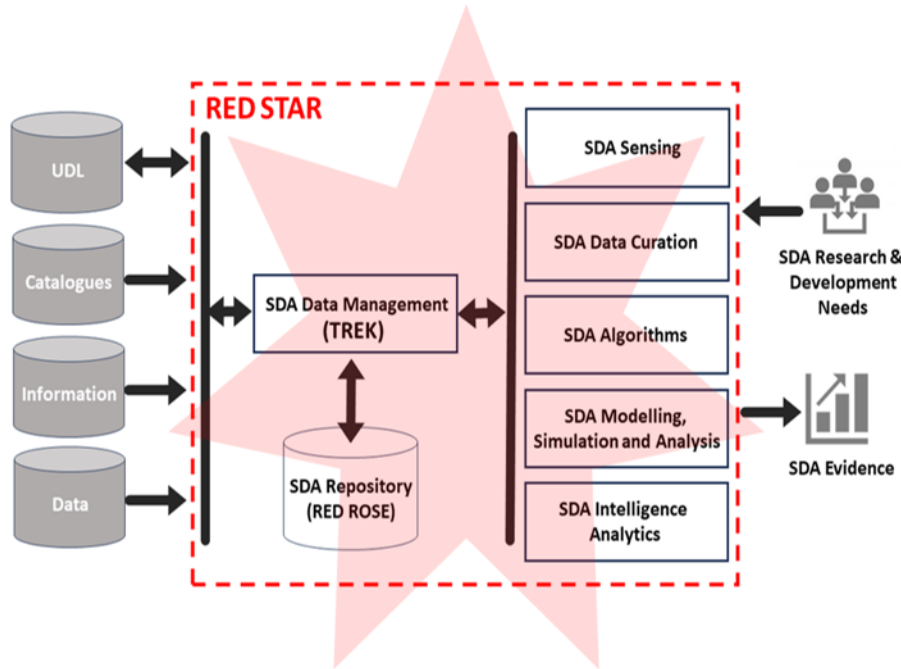


Figure 1. RED STAR architecture

### 3. SATELLITE MANOEUVRES

Satellites perform manoeuvres to ensure safety, comply with regulations and to fulfil their mission objectives. These manoeuvres typically involve adjusting velocity using on-board propulsion or other control systems and may be accompanied by changes in the satellite's attitude.

In LEO, manoeuvres are often necessary to counteract atmospheric drag, which causes gradual orbital decay. Satellites in large constellations like Starlink [13] or OneWeb, must frequently adjust their orbits to maintain precise spacing within their formations. Manoeuvres are also performed to avoid potential collisions with other satellites or debris, often in response to conjunction warnings issued by space surveillance networks. In GEO, where satellites are typically expected to hover over the same longitude, operators perform station-keeping manoeuvres to correct for natural drift in inclination and longitude caused by gravitational perturbations and solar radiation pressure (SRP). Other reasons for manoeuvring include orbit raising and de-orbiting at end of life, and in some cases, covert relocation or proximity operations, especially for Defence related missions.

The ability to detect a manoeuvre is a critical component of SDA. A manoeuvre, especially if unexpected or unannounced, may have implications for safety, operational planning, or even strategic threat assessment. For example, a satellite drifting away from its assigned GEO slot without notice may be experiencing a failure or executing a repositioning. Frequent small manoeuvres might indicate high-agility operations such as Rendezvous and Proximity Operations (RPO). It could also hint at the ability to rapidly change orbits and pose a threat to a variety of satellites. Detecting these manoeuvres enables space operators and analysts to update orbital states, avoid collisions with nearby

objects and understand events happening on-orbit. It also supports long-term catalogue health, as undetected manoeuvres can lead to misidentification or even loss of custody, where the satellite's orbital state becomes too inaccurate to be useful.

In addition to detecting that a satellite has performed a manoeuvre, it is important to estimate the resulting change in its velocity vector, the delta-V, which encompasses both the magnitude and direction of the applied impulse. Estimating delta-V provides insight into fuel usage, mission intent, and spacecraft capability. For example, a satellite that performs a large delta-V manoeuvre in GEO may be relocating to a new orbital slot, perhaps for commercial, regulatory, or strategic purposes. In military contexts, high frequency or high agility manoeuvres might suggest on-orbit inspection, shadowing, or evasion tactics. Precise delta-V estimation also enables analysts to model future manoeuvrability including assessing how much fuel may remain, and therefore how long a satellite may continue operating or posing a potential threat.

Detecting and characterising manoeuvres is inherently challenging. One of the main difficulties lies in the resolution and frequency of observations. Manoeuvres may be gradual or low thrust and changes can be difficult to distinguish from natural perturbations without continuous or frequent monitoring. Sparse observations, long revisit times, and sensor geometry limitations can result in uncertainty, particularly when manoeuvres are small or occur outside regular observation windows. Additionally, some manoeuvres are non-cooperative and deliberately obscure; military satellites may execute manoeuvres without public notice, cease broadcasting telemetry, or even attempt deception through feigned drift or intentional misidentification [14].

The increasing density of objects in Earth orbit amplifies the strategic value for monitoring satellite manoeuvres. From a civil space traffic management perspective, monitoring manoeuvres supports collision avoidance, enhances conjunction assessment accuracy and enables more efficient coordination of orbital operations. In Defence and intelligence sectors, manoeuvre monitoring is critical for identifying unexpected trajectory changes, characterising intent, assessing threat levels, and supporting attribution analysis. Ultimately, accurate detection and characterisation of satellite manoeuvres underpins effective governance frameworks, enables resilient space operations, and informs technical and policy responses in an increasingly contested and operationally complex space domain.

#### **4. MANOEUVRE DETECTION AND ESTIMATION ALGORITHM**

Space surveillance networks (SSNs) are systems of ground and space-based sensors, data processing centres, and operational frameworks designed to detect, track, identify, and catalogue objects in Earth orbit. These objects typically include active satellites, defunct satellites, rocket bodies, and debris. The primary goal of SSNs is to maintain awareness of entities in space to support safety, security, and sustainability of space operations. Examples of SSNs include; the US SSN which maintains public catalogue via space-track.org [15]; the European Space Surveillance and Tracking (EU SST) system [16]; the Russian International Scientific Optical Network (ISON) [17]; China's Space Situational Awareness (SSA) system [18]; and commercial systems such as those that contribute to the US JCO [19] and SDA TAP Lab [7, 8].

The goal of the work outlined in this paper is to accept data from an SSN, to detect satellite manoeuvres and, when manoeuvres are detected, to estimate the corresponding time and delta-V. The manoeuvre monitoring capability should be applicable to any orbital regime.

SDA sensor observations from an SSN typically comprise timestamped metric and magnitude components. Metric observations provide measurements of an object's position in space, relative to the observing sensor. Metric observations may include range, range-rate, time difference of arrival (TDOA), frequency difference of arrival (FDOA), and angle measurements such as Right Ascension (RA) and Declination (Dec) or azimuth and elevation. Magnitude observations measure the apparent brightness of an object, typically in the visible or infrared spectrum, and are related to the physical and reflective properties of the object, not its position.

A key function of an SSN is for cataloguing objects and estimating their orbits. Metric sensor observations are used to estimate orbits typically under the assumption that space objects undergo no manoeuvres. Two-Line Elements (TLEs) are a standardized data format used to describe the orbital parameters of Earth-orbiting objects. Each TLE

consists of two lines of text, encoding a compact summary of an object’s orbit at a specific epoch (reference time). TLEs are widely used for orbit propagation, especially with the Simplified General Perturbations 4 (SGP4) model.

In many cases satellites are non-cooperative and there is no prior information on manoeuvre times or capabilities. Manoeuvre detection and estimation is a widely published topic in the literature and can be broadly divided into three broad families of algorithms, as shown in Figure 2. The first type of algorithm is concerned with determining manoeuvres from metric sensor observations that have been processed into orbit estimates. Examples of this type of algorithm are those using TLEs to detect manoeuvres, see for example Shorten [20] which contains an excellent literature survey, or Pirovano [21] which links orbits calculated from short arcs of observations. The second type of algorithm in Figure 1 accepts metric sensor observations directly and incorporates manoeuvre detection and estimation as part of the orbit estimation process. The algorithm presented in this paper falls into this category. Both the first and second types could be referred to as ‘metric’ algorithms, which use observations of the object’s kinematics to deduce a manoeuvre. The third type of algorithm is based on other manoeuvre signatures that may be available from sensor observations, such as photometry from an optical sensor, or signal-to-noise ratio (SNR) from a radio-frequency (RF) sensor. Such magnitude data can reveal attitude changes, deployment events, or thruster firings that correlate with manoeuvres. An example of this type of algorithm can be found in Brown [22].

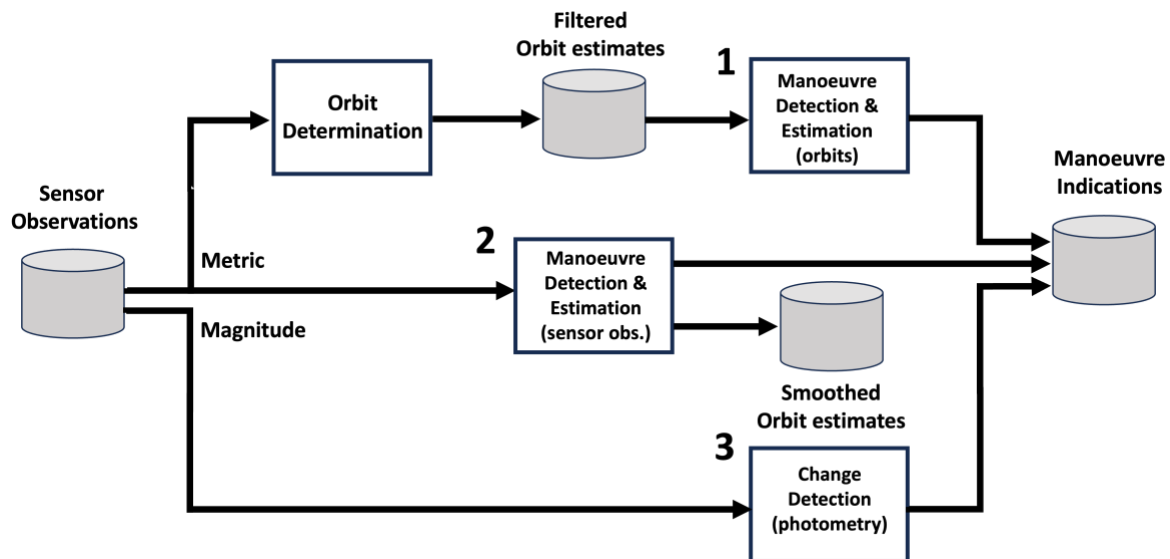


Figure 2. Three different approaches for satellite manoeuvre detection and estimation by processing: 1. orbit estimates; 2. metric sensor observations directly; and 3. the magnitude information of sensor observations

The manoeuvre detection and estimation algorithm presented in this paper builds on the ideas of Goff [23, 24] which shows the applicability of the interacting multiple-model (IMM) method for manoeuvre detection, and of Woodburn [25], which uses a backward smoother to estimate the parameters of an instantaneous manoeuvre. Our algorithm implements the generalised pseudo-Bayes order 2 (GPB2) algorithm [26, 27] in preference to the IMM, due to its slightly superior performance and simpler implementation, despite higher computational demands. Rather than smoothing backward with a single, no-manoeuve, model we smooth backwards with the full information provided by the Gaussian mixture of the multiple-model filter. The multiple-model smoother algorithm used is based on Barber’s expectation correction algorithm [13]. The implementation of the algorithm relies on the open-source Orekit astrodynamics library [28].

A significant feature of the algorithm presented here is that realistic uncertainties in the orbit state are maintained at all times, even during the manoeuvre, and that uncertainties in the estimated manoeuvre parameters (time and delta-V) are captured. Additionally, by designing the manoeuvre detection and estimation around a robust estimation process, the algorithm is independent of the sensor types, geometries and accuracies.

Figure 3 displays a flow-chart of the algorithm which can be divided into three phases:

- i. a detection phase, based on the forward estimation, which indicates a possible manoeuvre,
- ii. a bounding phase, using the filter (forward estimate) and smoother (backward estimate) to find a state before and after the manoeuvre, and
- iii. an estimation phase, which uses the bounding estimates to determine the time and change in velocity (delta-V) of the manoeuvre.

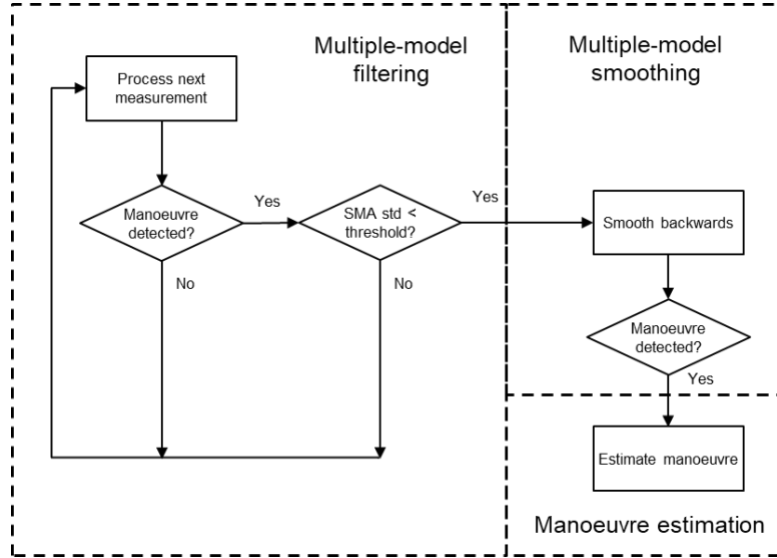


Figure 3. Flow-chart of the multiple-model manoeuvre detection and estimation algorithm.

More detail of each section of the algorithm is provided in the following sections. The multiple-model filtering algorithm – shown in the left-hand block of Figure 3 – processes sensor observations, calculating a state estimate (including covariance) and a probability of manoeuvre at each time-step. If the probability of manoeuvre exceeds a threshold (0.5 for this work) then the algorithm flags the possibility of a manoeuvre having occurred. While the filter keeps processing measurements, the estimated standard deviation (std. dev.) of the semi-major axis (SMA) is monitored. Once the std. dev. of the SMA has dropped to a satisfactory level, the manoeuvre estimation process is initiated, shown in the two right-hand blocks of Figure 3.

To estimate the time and delta-V of the manoeuvre we require a pre-manoeuve and post-manoeuve state including uncertainties. The pre-manoeuve state is extracted from the filter prior to the manoeuvre indication. The post-manoeuve state is calculated by backwards smoothing to just after the manoeuvre. Similar to the multiple-model filter, the multiple-model smoother indicates the smoothed probability of manoeuvre in addition to the orbital state. The algorithm uses the smoothed probability of manoeuvre to automatically determine a time after the manoeuvre and select a post-manoeuve state. Estimation of the manoeuvre parameters is performed using a least-squares method that minimises the manoeuvre delta-V, constrained by the pre- and post-manoeuve states.

#### 4.1 Multiple-Model Filtering

A multiple-model filtering algorithm is an approximate Bayesian estimation framework which automatically chooses one of a family of models that best matches the underlying data. The technique is commonly used in state-space estimation for change detection [29]. The mathematical representation of the system of models is known as jump-Markov systems, because the transitions between the models are defined probabilistically as a discrete Markov system. Details of the GPB2 algorithm that is used in this work and its relationship to the IMM can be found in Burke and Shorten [18, 13]. The most important feature is that at the end of an update step at time  $k$  the algorithm produces a state (mean,  $\hat{\mathbf{x}}_{k|k}^{(i)}$ , and covariance,  $P_{k|k}^{(i)}$ ) and a probability/weight,  $w_{k|k}^{(i)}$ , for each model  $i$ :

$$\hat{\mathbf{x}}_{k|k}^{(i)}, P_{k|k}^{(i)}, w_{k|k}^{(i)}$$

where the weights sum to unity. When a model (model 2, say) is a better match to the data, then  $w_{k|k}^{(2)}$  is close to one, whereas if the first model is a better match, then  $w_{k|k}^{(1)}$  is close to one. The model probabilities evolve over time and can be used to indicate the probability of a change after every measurement update. The overall estimate at each time is the Gaussian distribution which is moment-matched to the weighted Gaussian mixture:

$$\hat{x}_{k|k} = \sum_i w_{k|k}^{(i)} \hat{x}_{k|k}^{(i)}$$

$$P_{k|k} = \sum_i w_{k|k}^{(i)} \left\{ P_{k|k}^{(i)} + (\hat{x}_{k|k} - \hat{x}_{k|k}^{(i)})(\hat{x}_{k|k} - \hat{x}_{k|k}^{(i)})^T \right\}.$$

For the spacecraft manoeuvre detection algorithm, we have two different state transition models: one is a non-maneuvring model, and one represents in-track (East-West) manoeuvres. The two models use the same force models and orbital dynamics and only differ in the process noise added in the prediction phase of the estimation. Both models have a small amount of process noise to allow for unmodelled forces. This component of process noise scales with the time between measurements. The manoeuvre model introduces an additional, constant and time-independent, component of process noise which allows for a much larger in-track uncertainty in position and radial uncertainty in velocity.

The multiple-model filtering implementation uses a bank of extended Kalman filters (EKF) to estimate the six equinoctial orbital elements and solar radiation pressure (SRP), resulting in a seven-dimensional state. While the state is defined in equinoctial orbital elements, the state-dependent process noise is defined in Cartesian coordinates in a local orbital frame (Velocity-Normal-Conormal – VNC) and transformed into orbital elements.

## 4.2 Bounding the Manoeuvre

The manoeuvre estimation process described in the next section requires a state (mean and covariance) before and after the manoeuvre. We will refer to these as the pre- and post-manoevrue states, or bounding states. Since the uncertainty in the estimated parameters will reflect the uncertainty in the bounding states, it is desirable to provide the estimator with as precise orbit estimates as possible.

As explored by Goff [23], a multiple-model filtering algorithm can track through a manoeuvre, providing estimates at every time-step that are consistent with the measurements. The effect of a model with large process noise is that the covariance of the estimate inflates significantly, so that in situations where the manoeuvre model has a high probability the covariance of the estimate will be much larger than the covariance before the manoeuvre.

The method used in this work to counter the inflation in the estimate's covariance is to allow additional time to pass. As more measurements are provided to the filter after the manoeuvre, the covariance will reduce and gradually converge to its pre-manoevrue level. We can then use a smoother to run backward over the states, maintaining accuracy, until just after the manoeuvre. By using a multiple-model smoother [30] we are provided with a smoothed state and a smoothed probability of manoeuvre. The smoothed probability of manoeuvre indicates when the manoeuvre occurred, allowing us to choose a time just after the likely time of the manoeuvre. The smoothed state gives a more accurate post-manoevrue state compared to that provided by the filter.

An example of this process is shown in Figure 4, which shows the uncertainty (estimated standard deviation) of the semi-major axis (SMA) over time around a manoeuvre and the model probabilities from the filter and smoother around the same event. Figure 3 shows that the uncertainty spikes after the manoeuvre due to the large process noise introduced by the manoeuvre model and as more measurements are processed the uncertainty reduces. At the same time the manoeuvre probability increases after the manoeuvre and reduces almost immediately after the initial manoeuvre indication.

Once the uncertainty in SMA drops below a threshold (we use a multiple of the pre-manoevrue uncertainty), the multiple-model smoothing process is initiated. Note that the longer we wait, the more accurate the smoothed estimate will be just after the manoeuvre. A compromise needs to be made between the time delay that is acceptable to the user and the accuracy required of the manoeuvre parameters. As expected from multiple model smoothing, the

uncertainty of the smoothed estimate grows around the time of the manoeuvre, shown in Figure 4, along with the smoothed manoeuvre probability.

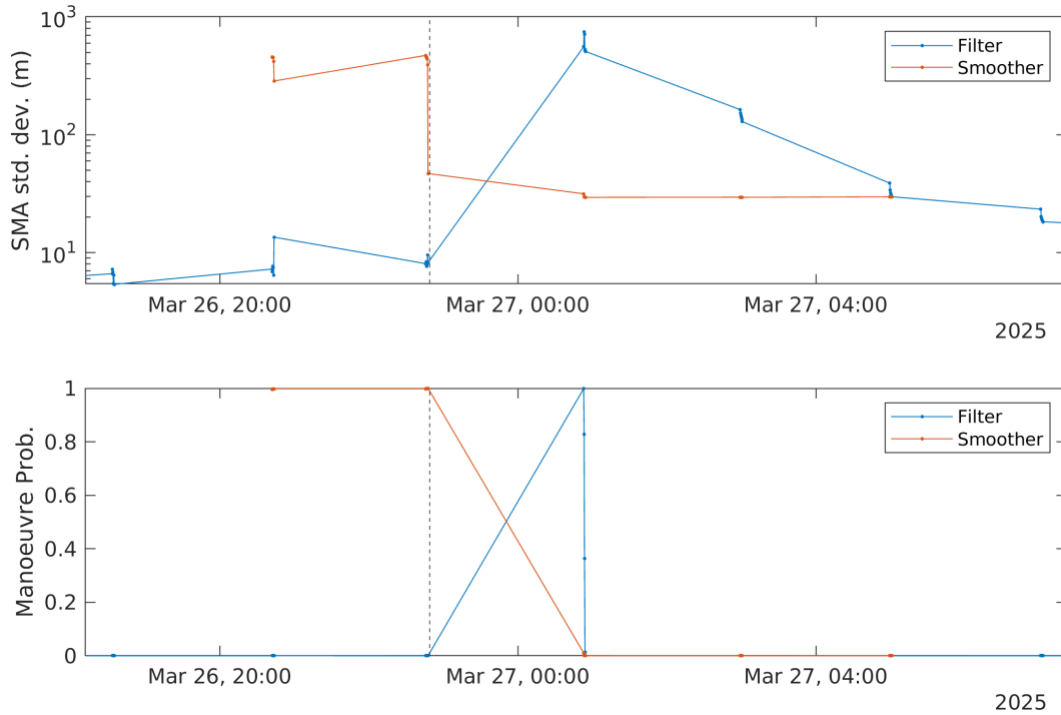


Figure 4. The top plot shows the uncertainty in semi-major axis (SMA) over a manoeuvre for both the multiple-model filter (forward estimator) in blue and smoother (backward estimator) in orange. The lower plot shows manoeuvre probability calculated by the filter.

The combination of manoeuvre indication from the multiple-model filter running forward in time, and the multiple-model smoother running backward in time, gives us a reliable method of choosing times that bound the manoeuvre. In the forward direction a time and corresponding orbital state is chosen just before the filter’s manoeuvre indication, providing a pre-manoeuve state. Similarly, in the backward direction a time and orbital state is chosen just after the smoother manoeuvre probability increases. Together these supply accurate estimates of the bounding states required for estimating the manoeuvre parameters.

### 4.3 Estimating the Manoeuvre Parameters

As described in the previous section the forward filter provides a mean and covariance of the state before the manoeuvre and the backward smoother provides a mean and covariance of the state after the manoeuvre. Given the bounding states we can use a standard least-squares algorithm to determine the manoeuvre parameters, along with a lower-bound on the uncertainty.

Figure 5 is a conceptual diagram showing the geometry of the estimation problem. The bounding states (mean, covariance and time) are known, and the time and delta-V of the manoeuvre are the quantities that need to be inferred. This can be intuitively understood as supplying two position/velocity “measurements” (with value and noise covariance given by the filter/smoother estimates) to a least-squares algorithm, which estimates the manoeuvre parameters subject to minimising the delta-V.

There is some subtlety for this problem, in that the estimated trajectory will have a discontinuous jump in velocity at the manoeuvre time but must remain continuous in position. That implies that fixing the trajectory to the mean of the bounding states would be too restrictive and give unrealistic results. To provide some flexibility, within the constraints of the bounding states, we estimate the following seven parameters:

- Post-manoeuve velocity, constrained by the smoother covariance (3 parameters)
- Time since pre-manoeuve estimate (1 parameter)
- Change in velocity, delta-V, in the relative VNC local orbital frame (3 parameters)

This implies that the pre-manoeuve position and velocity are fixed, along with the post-manoeuve position, but the post-manoeuve velocity is allowed to vary, within the constraints of the covariance. The result from the least-squares algorithm gives an estimate of these seven parameters, along with a covariance matrix, which captures the uncertainty in the bounding states.

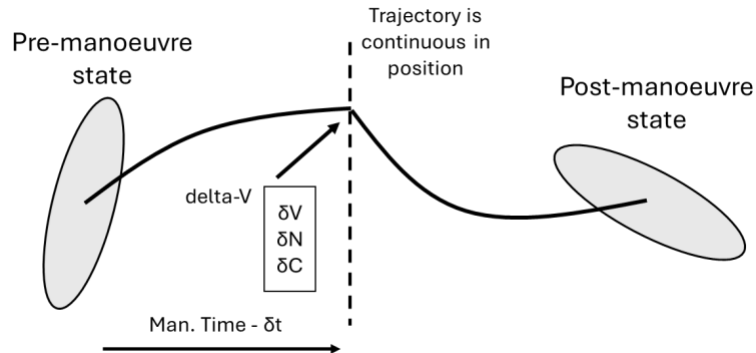


Figure 5. Conceptual diagram of the estimated manoeuvre quantities; time relative to the pre-manoeuve state and delta-V (in Velocity-Normal-Conormal coordinates).

## 5. SIMULATION EXAMPLE

A simulated scenario comprising manoeuvring satellites was developed in order to evaluate the manoeuvre detection and estimation algorithm. The details of the simulation example are described in this section of the paper.

A GEO station-keeping satellite was chosen for the simulation example as a representative manoeuvre detection and estimation problem for SDA as most GEO satellites will do periodic orbit maintenance manoeuvres. These manoeuvres are increasingly difficult to detect and even more difficult to estimate as hybrid satellites (where both chemical and electric thrusters are on-board) become more common. The magnitude of East-West station-keeping manoeuvres for geostationary and geosynchronous satellites are on the order of centimetres per second meaning this also poses a somewhat challenging scenario for the algorithm compared to larger, more noticeable burns.

Three independent satellites in GEO were simulated for a duration of one year with the satellites performing manoeuvres to ensure they remained on their respective stations. The three satellites were labelled to correspond with the American comedy troupe, the three Stooges, namely Moe, Larry and, Curly, which were assigned longitude ‘slots’ of  $164^\circ$ ,  $167^\circ$  and  $170^\circ$  East, respectively. The trajectory of each of the satellites were initiated with arbitrary East - West motion relative to their individual longitude slot and with zero inclination. East-West manoeuvres were simulated to maintain the satellite’s position to within 0.1 degree of the assigned longitude. No North-South manoeuvres were simulated and so the inclination of each satellite was unconstrained for the duration of the simulation. Systems Tool Kit (STK) was used to propagate and manoeuvre the satellites with manoeuvres occurring when the eastern or western boundary of the longitude box was breached by the next nodal crossing. This means that there could be some time where a satellite was outside of its GEO box but the duration was limited to less than half the orbital period of the satellite. Figure 6 shows the three satellites and their corresponding GEO boxes positioned above the Pacific Ocean near the Kwajalein Atoll in the Marshall Islands, located at latitude  $8^\circ 43'N$  and longitude  $167^\circ 44'E$ .

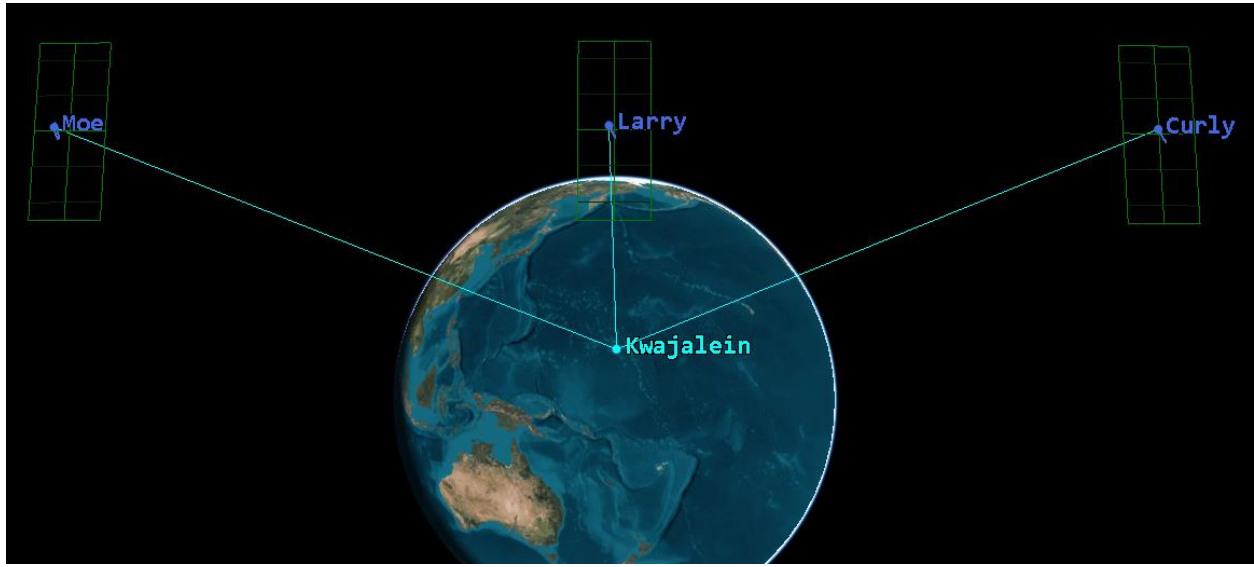


Figure 6. Visualisation of the three simulated satellites Moe, Larry and Curly with their geostationary box. The simulated sensor at Kwajalein is seen on the surface of the Earth

The manoeuvre methodology utilised the natural longitudinal drift of geostationary satellites. For East-West variations the main perturbations are the tesseral terms of the Earth's gravitational field, namely J21, J22, J33 and J44, as well as the SRP that varies throughout the year [31]. Since the satellites are located between 160° and 170° East, the natural drift of all three satellites was in the easterly direction. As shown in Figure 7 the manoeuvres occurred on the eastern boundary of the GEO box and therefore required a positive in-track delta-V which could be calculated to just touch the western boundary before naturally drifting back towards the eastern boundary.

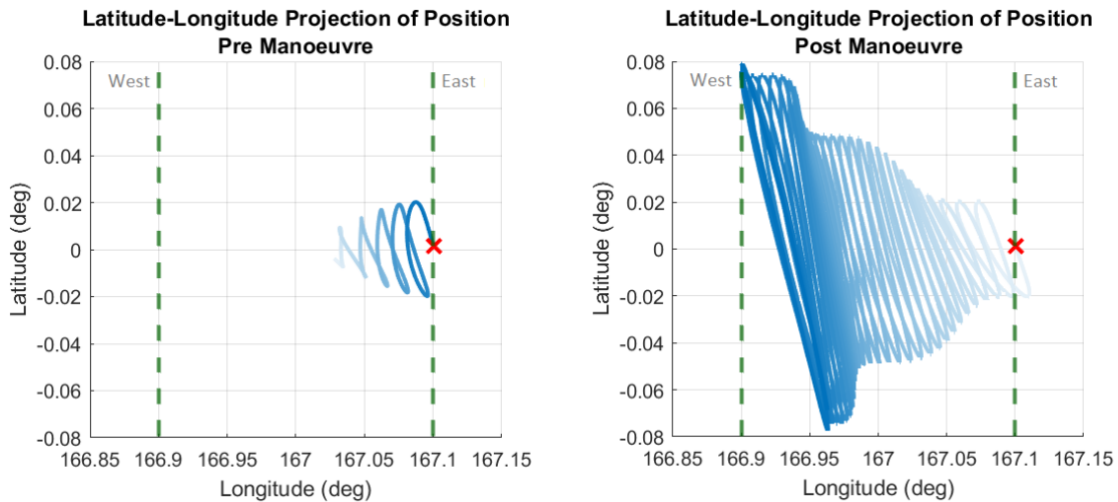


Figure 7. Latitude – Longitude positions of the Larry satellite before (left) and after (right) a station-keeping manoeuvre. The green vertical dashed lines indicate the longitude boundary for the station. The blue line shows the satellite position with the passage of time depicted by the darkening of the line. The red crosses depict where the simulated manoeuvre is applied as the next nodal crossing is outside the eastern boundary.

Metric sensor observations were simulated from a notional ground-based radar at Kwajalein, which is the location of several operational radar installations for space surveillance [32]. The trajectory, or ephemeris, data from each of the simulated satellites was passed into a script that calculated the cadence and geometries for each sensor observation.

The cadence of the sensor observations is shown in Figure 8 with each observation consisting of its time stamp, azimuth, elevation and range components. Each of the sensor observations had a random error applied to it with zero mean with a standard deviation for each component that is representative of a ground-based SDA radar system. All observations considered appropriate physical phenomena (such as light-time), so that the manoeuvre detection and estimation algorithm should require minimal changes when being applied to real data [33].

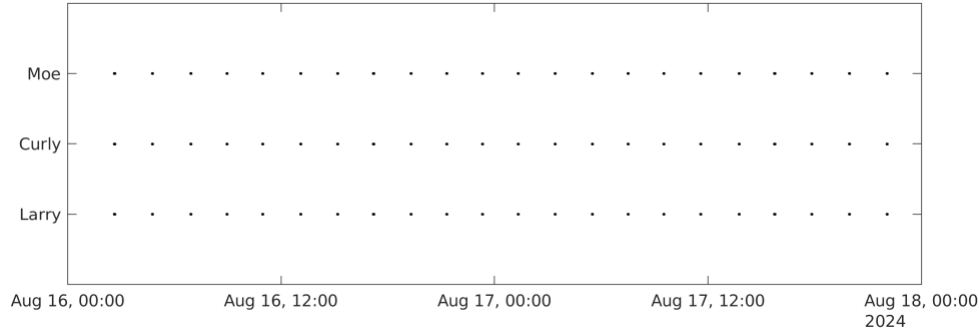


Figure 8. The observation times for each of the simulated satellites. Each dot represents a simulated observation, generated in groups of six spaced 20 seconds apart, with each group occurring approximately every two hours.

## 6. MANOEUVRE DETECTION AND ESTIMATION RESULTS

This section summarises the results of the multiple-model manoeuvre detection and estimation algorithm applied to the three simulated data sets described in the previous section. While orbital estimation accuracy is critical, these results focus on the timeliness and accuracy of the manoeuvre detection and estimation parts of the algorithm.

Figure 9, Figure 10 and Figure 11 summarise the output of the algorithm for the three satellites. The geodetic longitude, computed from the mean of the orbital estimate at each time, clearly shows that the satellites manoeuvre to stay within their assigned longitude slots over the full duration of the simulation. The peaks in the estimates at the top of each plot (maximum longitude) indicate where the satellite has needed to manoeuvre to stay within its slot. The manoeuvre probability shows the probability of the manoeuvre model in the multiple-model filter. This quantity is used to indicate a manoeuvre and trigger the manoeuvre estimation process. The spikes in manoeuvre probability correspond to the peaks in the longitude plot, showing that the algorithm reliably detects each manoeuvre. It is interesting to note that the simulations have each satellite performing manoeuvres at different rates, with Larry (Figure 10), requiring nine manoeuvres, Curly (Figure 11) requiring ten and Moe (Figure 9) requiring only four. The algorithm can automatically detect and estimate the manoeuvres in each case despite the different orbit maintenance strategies.

The manoeuvre probability plots in Figure 9, Figure 10 and Figure 11 additionally contain red diamond-shaped markers corresponding to the estimated manoeuvre time from the full estimation process. Most of the spikes in manoeuvre probability are overlaid with a marker, with some exceptions. Both Larry (Figure 10) and Moe (Figure 9) have a spike at the beginning of the estimation process, where the estimator falsely indicates a manoeuvre. These two spikes aren't unexpected, since they occur as the estimator is transitioning from an initial state, with initially conservative (large) covariance, to converge on a state driven by the measurements. The manoeuvre estimation algorithm correctly identifies these as false manoeuvre indications. There is a single manoeuvre indication (the 5<sup>th</sup> manoeuvre of Larry) where the manoeuvre estimation process failed. More work is required to understand the reasons for this failure.

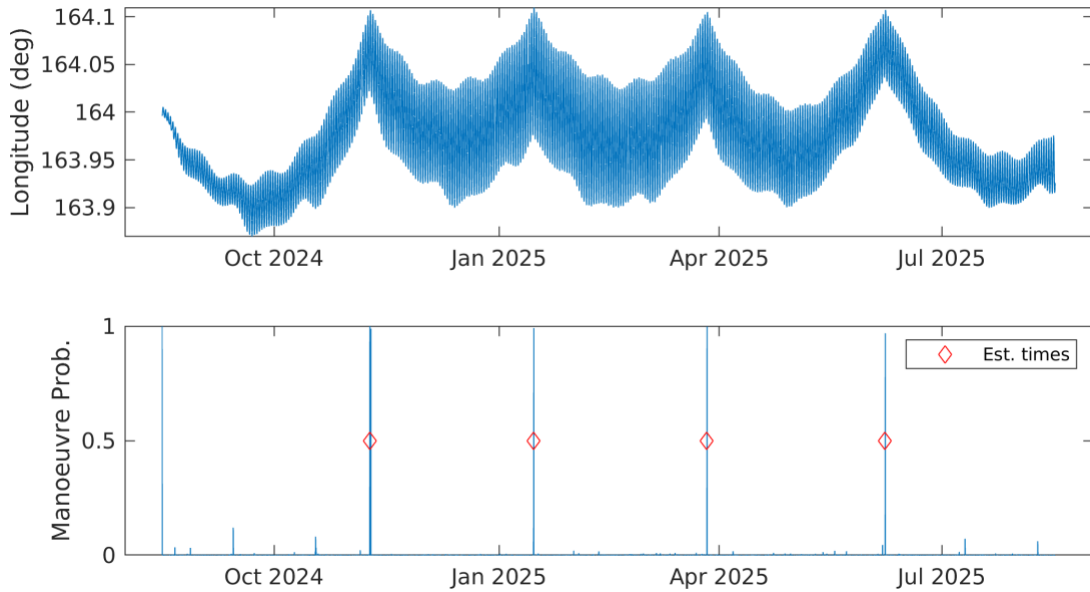


Figure 9. Moe. The top plot shows the estimated longitude over time, while the lower plot shows the manoeuvre probability over time. Red diamonds mark the estimated manoeuvre times.

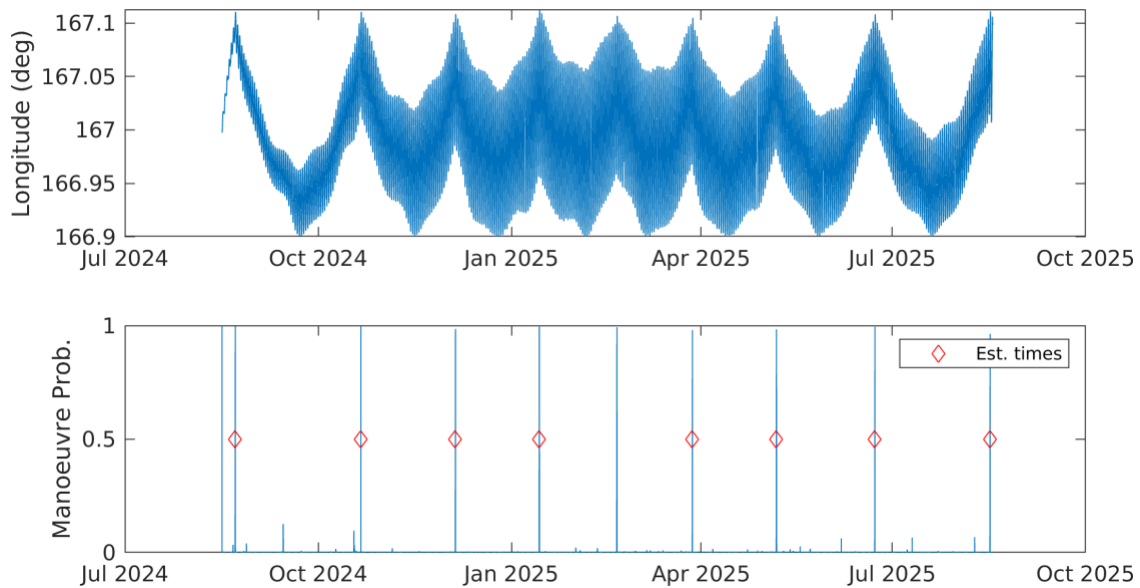


Figure 10. Larry. The top plot shows the estimated longitude over time, while the lower plot shows the manoeuvre probability over time. Red diamonds mark the estimated manoeuvre times. Note that, while the probability clearly indicates a manoeuvre, the manoeuvre estimation calculations failed for the manoeuvre of March 2025.

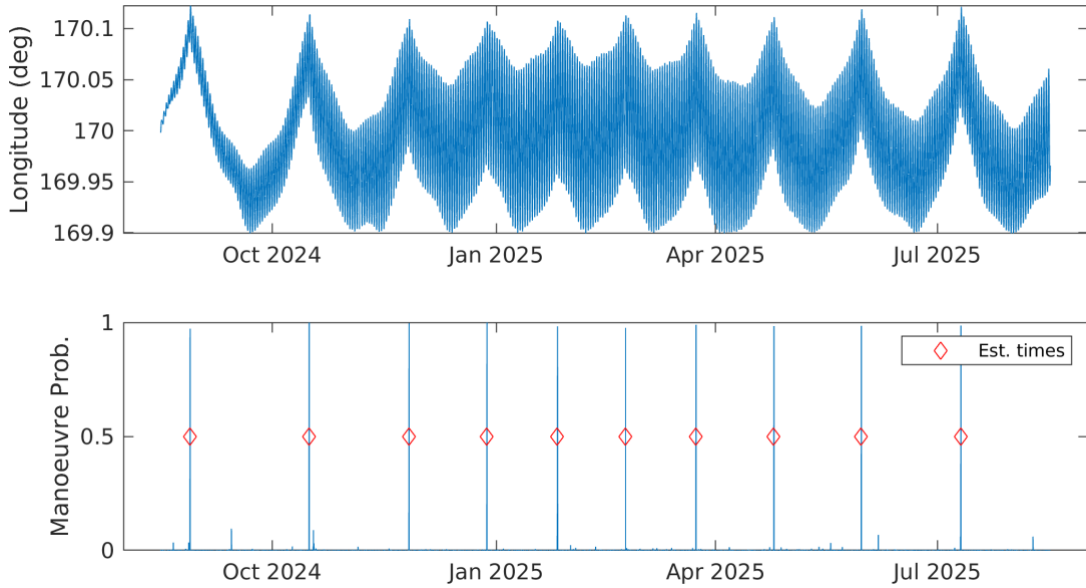


Figure 11. Curly. The top plot shows the estimated longitude over time, while the lower plot shows the manoeuvre probability over time. Red diamonds mark the estimated manoeuvre times.

An accuracy comparison of the estimated manoeuvre quantities is shown in Figure 12, with results combined for all three simulated objects. The plot shows the error in in-track delta-V (only the “V” component in the VNC-calculated delta-V) compared to ground-truth and the error in the estimated manoeuvre time, compared to ground-truth. Most of the estimates are within an hour from the true time of the manoeuvre and within a few mm/s for the estimated delta-V. As described in the previous section the magnitude of the East-West orbit maintenance manoeuvres for these objects are in the order of cm/s, implying that these estimates are within roughly 10% of the true delta-V. We can see that there is a slight bias, with the estimated manoeuvre time being slightly early and the estimated delta-V being slightly under-estimated. The right-hand plot in Figure 12 shows the differences normalised by the estimated error standard deviation, showing that the estimate covariance is consistent with the errors in the mean, although slightly pessimistic in delta-V. The last three manoeuvres performed by Curly resulted in large deviations (greater than 24 hours) from the true manoeuvre time and are not shown in the plot. More work is required to understand why the estimation process performed poorly for those manoeuvres.

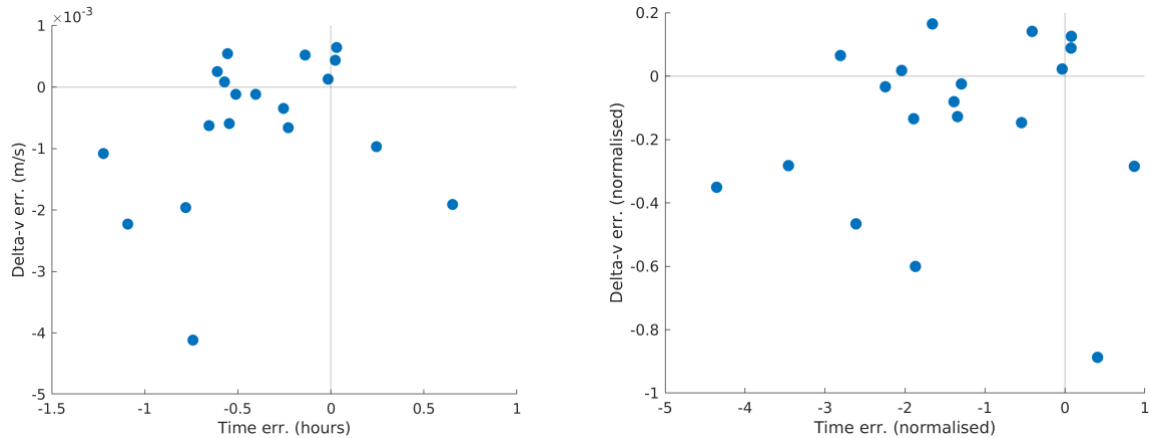


Figure 12. Differences between the true and estimated times and delta-V for each manoeuvre. The left plot shows the differences in natural units, while the right plot shows the differences normalised by the estimate’s error standard deviation.

The algorithm, as described in Section 3, aims to declare a manoeuvre as soon as possible after the event, then delay until there is enough information to reliably estimate the parameters of the manoeuvre. Figure 13 summarises each of these delays for the combined manoeuvres of the three satellites as two histograms. We can see that the manoeuvre

events are all detected within four hours, which corresponds to at most two observation periods in our simulation. The delay until the backward smoothing process is triggered is typically less than twelve hours after the manoeuvre. We should note that these timelines are highly dependent on the sensor data available and could change dramatically with different sensor types, geometries and observation cadence.

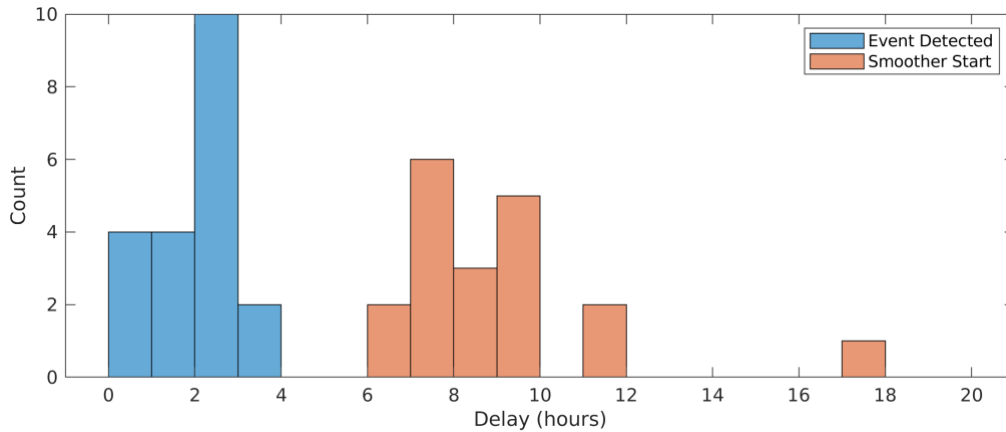


Figure 13. Histogram of time delay for detection of a manoeuvre (blue) and for manoeuvre estimation (orange.)

This section presented results of the manoeuvre detection and estimation algorithm applied to sensor observation data from a simulated ground-based radar observing simulated satellite manoeuvres. The manoeuvre detection and estimation algorithm has also been applied to observation data from real sensors observing real satellite manoeuvres. The type of sensors tested included ground-based radar, ground-based optical, space-based optical and Passive RF. Preliminary results for satellites performing manoeuvres in GEO indicate similar performance to that presented in this paper. Further investigations are required, but early findings suggest that the algorithm presented in this paper shows promise as an option for satellite manoeuvre detection and estimation.

## 7. CONCLUSIONS

This work presents a manoeuvre detection and estimation algorithm developed by the Defence Science and Technology Group (DSTG) as part of Australia’s RED STAR experimental space domain awareness system. The algorithm addresses the challenge of detecting and characterising uncooperative satellite manoeuvres, particularly in the geosynchronous regime where sparse observations and small delta-V values complicate tracking. A key contribution is the use of a multiple-model filtering and smoothing approach that maintains realistic orbit uncertainties, enabling robust estimation of manoeuvre parameters, including time and delta-V, without requiring prior knowledge of the manoeuvre.

The approach for manoeuvre detection and estimation is designed to be sensor-agnostic but further testing is required to consider multiple types of input data. For the simulation considered in this paper, the scenario was limited to data from simulated ground-based radar observations of three GEO satellites performing East–West station-keeping manoeuvres. Each satellite’s trajectory was monitored with observations approximately every two hours with the algorithm automatically identifying and estimating most manoeuvres. Results show good agreement between estimated and true manoeuvre characteristics, with detection delays typically under four hours and delta-V estimates accurate to within 10% of truth, demonstrating the algorithm’s potential for operational relevance.

This paper highlights the importance of accurate manoeuvre detection in a modern space surveillance context. As the number of satellites increases, the ability to detect and characterise unexpected orbital changes will be essential for catalogue maintenance, conjunction assessment, attribution, and security. By exploiting both metric observations and a Bayesian estimation framework, the DSTG algorithm provides a foundation for Australia’s future SDA system acquisitions.

More broadly, the RED STAR system demonstrates a modular, data-driven approach to SDA research and prototyping. Its integration of simulation, data curation, and algorithmic analysis within a containerised architecture ensures flexibility across sensor types and orbital regimes. The manoeuvre detection algorithm presented here contributes to this capability, offering a tool that can improve situational awareness in the increasingly congested and contested space environment.

## 8. ACKNOWLEDGEMENT

This work was conducted as part of a research contract between the Defence Science and Technology Group and Qinetiq Australia, which subcontracted In Track Solutions.

## 9. REFERENCES

- [1] -, Australia's Space Surveillance Radar reaches Full Operational Capability, Defence Media release, 7 March 2017
- [2] -, Space surveillance telescope is declared operational, Defence Media release, 30 September 2022
- [3] -, New Defence space capability boosts regional security, Defence Media release, 2 December 2023
- [4] L. Sodders, Deep Space Advanced Radar Capability makes tremendous progress in first year, <https://www.spaceforce.mil/news/article-display/article/4072069/deep-space-advanced-radar-capability-makes-tremendous-progress-in-first-year/>, 20 February 2025 (accessed 22 July 2025)
- [5] -, Following the sun for space domain awareness, <https://www.defence.gov.au/news-events/news/2023-09-01/following-sun-space-domain-awareness>, 1 September 2023
- [6] J.D. Gerber, Y. Picard, M. Brown, J. Held, F. Pelletier, T. Fuller, Sprint Advanced Concept Training (SACT): A renaissance in collaborative international space operations, AMOS 2020
- [7] S.P. Allen, SDA TAP Lab Using Commercial Technology to Avoid Operational Surprise, AMOS 2024
- [8] G. Furlich, A. Crews, J. McGuigan, T. McLaughlin, C. Burns, P. Balster, G. Jones, G. Hofer, I.S. Bartlett, L. Hettiarachchi, H. Spolar, S.P. Allen. Automated, Collaborative Applications to Close Kill-chain Gaps, AMOS 2024
- [9] -, Commercial space operations technologies tested in real-world environment, <https://www.space.gov.au/news-and-media/commercial-space-operations-technologies-tested-real-world-environment>, 26 July 2023 (accessed 22 July 2025)
- [10] -, Defence nanosatellite launched into orbit, Defence Media release, 18 March 2025
- [11] -. New era in Defence satellite communications research, Defence Media release, 28 June 2021
- [12] K. White, D. Cook, S. Kharabash, A. Kumar, V. Fok, C. Webb, P. Bawden, J. Alvino, H. Gaetjens, K. See, T. Jansen-Sturgeon, J. Barr, F. Piragibe de Almeida, M. Rutten, An Australian experimental SDA system: RED STAR, AMOS 2024
- [13] D.P. Shorten, W. Karunarathne and M. Roughan. How Is Starlink Manoeuvring? An Analysis of Patterns in the Manoeuvres of Starlink Satellites, In Proceedings of the 9th International Conference on Internet of Things, Big Data and Security, pages 174-184, 2024.
- [14] C. Colins. (2021 October 28). US, China, Russia Test New Space War Tactics: Sats Buzzing, Spoofing, Spying *Breaking Defence* ([US, China, Russia Test New Space War Tactics: Sats Buzzing, Spoofing, Spying - Breaking Defence](#))
- [15] -, space-track.org, <https://www.space-track.org/>
- [16] -, European Union Agency for the Space Programme, European Union Space Surveillance and Tracking, <https://www.euspa.europa.eu/eu-space-programme/ssa/eu-sst>
- [17] -, Site of initiative astronomical projects: International Scientific Optical Network (ISON) & Low Frequency VLBI Network (LFVN), <http://lfvn.astronomer.ru/main/english.htm>
- [18] K. Burke, China's Different Approach to Space Situational Awareness, China Aerospace Studies Institute, December 2024
- [19] B. Golf, A. Konnath, Joint Commercial Operations (JCO) Introduction and Way Forward, AMOS, 2024.
- [20] D.P. Shorten, M. Humphries, J. Maclean, Y. Yang and M. Roughan, "Optimal Proposal Particle Filters for Detecting Anomalies and Manoeuvres from Two Line Element Data", *Acta Astronautica* 228: 709–23, 2025
- [21] L. Pirovano and R. Armellini, "Detection and Estimation of Spacecraft Maneuvers for Catalog Maintenance", *Acta Astronautica* 215: 387–97, February 2024

- [22] M. Brown, B. Smith, C. Capon, R. Abay, M. Cegarra Polo, S. Gehly, G. Bowden, C. Bright, A. Lambert, R. Boyce, SSA Experiments for the Australian M2 Formation Flying CubeSat Mission, AMOS 2020
- [23] G.M. Goff, Orbit Estimation of Non-Cooperative Maneuvering Spacecraft, PhD thesis, Air Force Institute of Technology, Wright-Patterson Air Force Base, Ohio, USA, 2015
- [24] G.M. Goff, J.T. Black and J.A. Beck. "Tracking Maneuvering Spacecraft with Filter-through Approaches Using Interacting Multiple Models." *Acta Astronautica* 114, 152–63, September 2015
- [25] J. Woodburn, J. Carrico, J.R. Wright, Estimation of instantaneous maneuvers using a fixed interval smoother, *Adv. Astronaut. Sci.* 116: 243–260, 2003
- [26] Y. Bar-Shalom, P. Willett, and X. Tian. Tracking and Data Fusion: A Handbook of Algorithms. YBS Publishing, April 2011
- [27] S. Blackman, R. Popoli, *Design and Analysis of Modern Tracking Systems,* Artech House, Norwood, 1999
- [28] CS-SI/Orekit. <https://doi.org/10.5281/zenodo.7249096>
- [29] F. Gustafsson, *Adaptive Filtering and Change Detection.* John Wiley & Sons, Ltd, 2001
- [30] David Barber. *Bayesian Reasoning and Machine Learning.* Cambridge University Press, 1 edition, June 2012
- [31] H. Li, Maintaining Geostationary Orbit, *Geostationary Satellites Collocation.* Springer, 2014
- [32] J. A. Nelson and K. R. Roth, History of Lincoln Laboratory at the Reagan Test Site, Lincoln Laboratory Journal, Volume 19, Number 2, 2012
- [33] D. A. Vallado, *Fundamentals of Astrodynamics and Applications,* Fifth Edition, Microcosm Press, 2022